Supplementary Online Material (SOM):

Finite element analysis of Neanderthal and early *Homo sapiens* maxillary central incisor

Ali Najafzadeh[a,b,1], María Hernaiz-García[a,1], Stefano Benazzi[c], Bernard Chen[d], Jean-Jacques Hublin[e,f], Ottmar Kullmer[g,h], Ariel Pokhojaev[i], Rachel Sarig[i,j], Rita Sorrentino[c,k], Antonino Vazzana[c], Luca Fiorenza[a,*]

[a] *Monash Biomedicine Discovery Institute, Department of Anatomy and Developmental Biology, Monash University, Melbourne, VIC 3800, Australia*

[b] *Department of Mechanical and Aerospace Engineering, Monash University, Melbourne, VIC 3800, Australia*

[c] *Department of Cultural Heritage, University of Bologna, Ravenna 48121, Italy*

[d] *Department of Surgery, The University of Melbourne, Melbourne, VIC 3010, Australia*

[e] *Chaire de Paléoanthropologie, CIRB (UMR 7241-U1050), Collège de France, 11, Place Marcelin-Berthelot, 75231 Paris, Cedex 05, France*

[f] *Max Planck Institute for Evolutionary Anthropology, Leipzig 04103, Germany*

[g] *Division of Palaeoanthropology, Senckenberg Research Institute and Natural History Museum Frankfurt, Frankfurt a. M. 60325, Germany*

[h] *Department of Palaeobiology and Environment, Institute of Ecology, Evolution, and Diversity, Goethe University, Frankfurt a. M. 60438, Germany*

[i] *Department of Oral Biology, The Goldschleger School of Dental Medicine, Sackler Faculty of Medicine, Tel Aviv University, Tel Aviv 69978, Israel*

[j] *Dan David Center for Human Evolution and Biohistory Research, Sackler Faculty of Medicine, Tel Aviv University, Tel Aviv 69978, Israel*

[k] *Department of Biological, Geological and Environmental Sciences, University of Bologna, Bologna 40126, Italy*

[1] The first two authors contributed equally to this work.

*** Corresponding author.**

E-mail address: luca.fiorenza@monash.edu (L. Fiorenza).

SOM Figure S1. Le Moustier 1 original skeletal remains showing the skull fragments, the maxilla and the mandible.

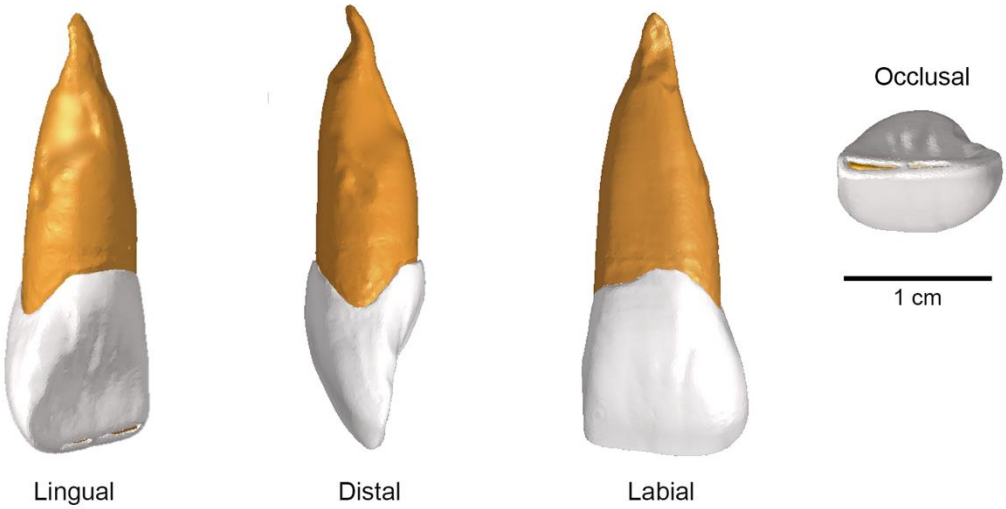

SOM Figure S2. Three-dimensional (3D) digital models of Qafzeh 9 maxillary left I^1 in lingual, distal, labial and occlusal views.

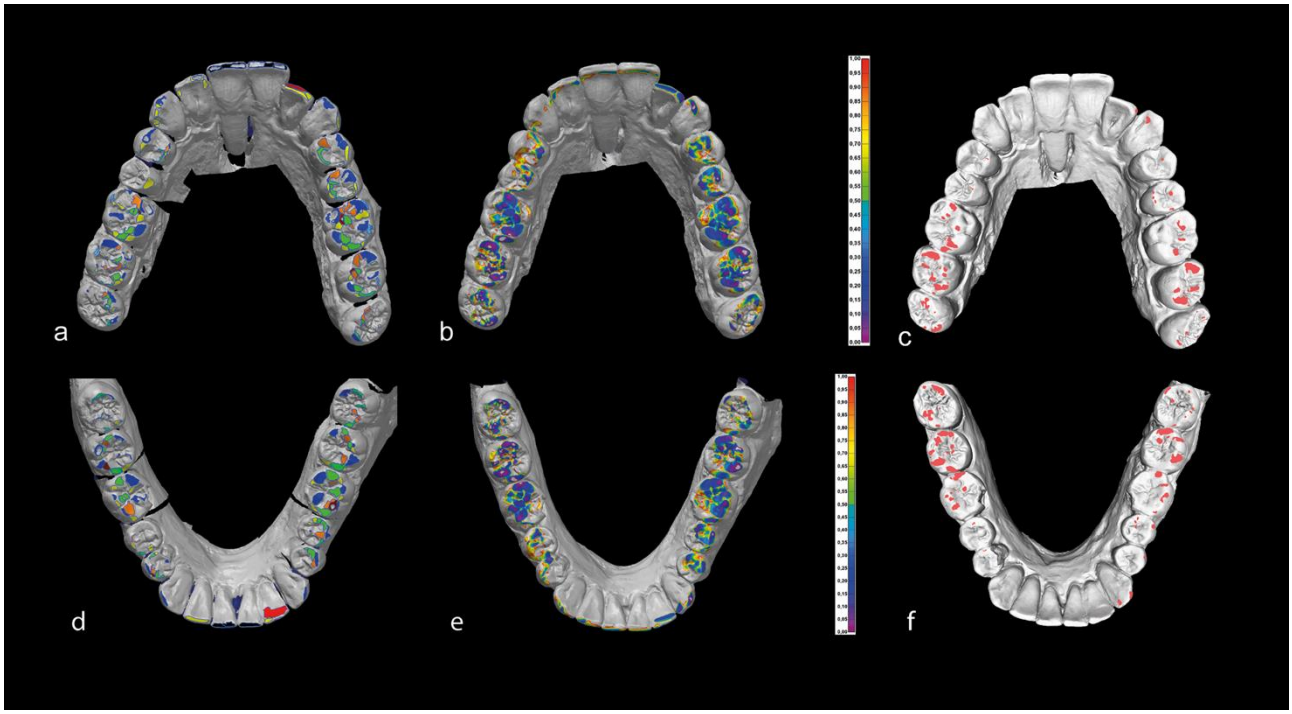

SOM Figure S3. Color-coded wear facet maps of the reconstructed Qafzeh 9 dental arches following the concept of the occlusal fingerprint analysis (Kullmer et al. 2009; a and d). Color maps showing the deviation in maximum intercuspation occlusion (b and e). Purple and blue colors reflect full occlusal contacts at the locations wear facets. Occlusal contact maps obtained through the occlusal fingerprint analyzer software collision detection matching with the static occlusion of the physical reconstruction (c and f).

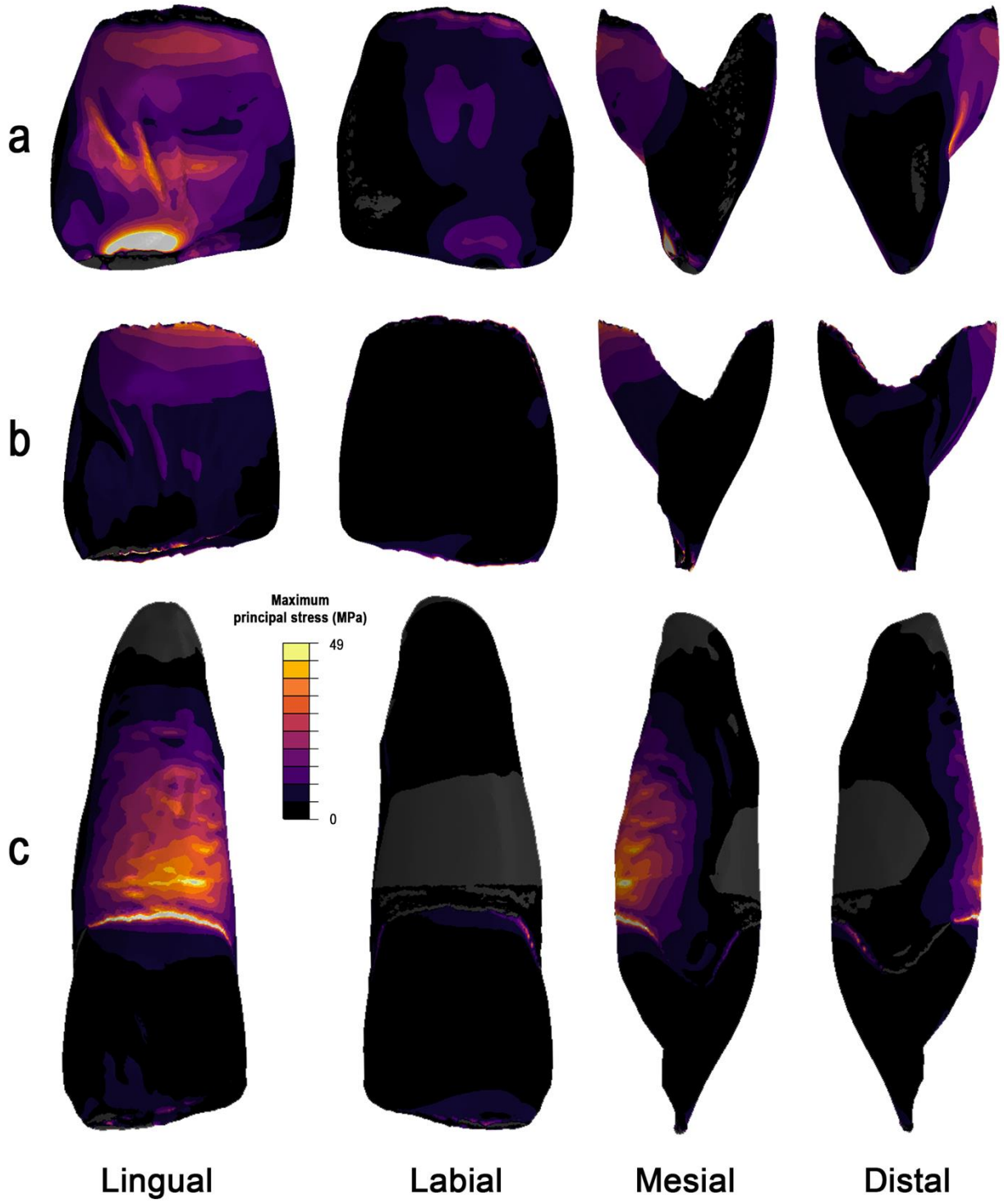

SOM Figure S4. 'Inferno' color maps showing the maximum principal stress distribution (MPa) of Le Moustier 1 left I^1 in lingual, labial, mesial and distal view during edge-to-edge occlusion (applied force = 294.4 N). Enamel (a), enamel-dentine junction (b) and dentine (c).

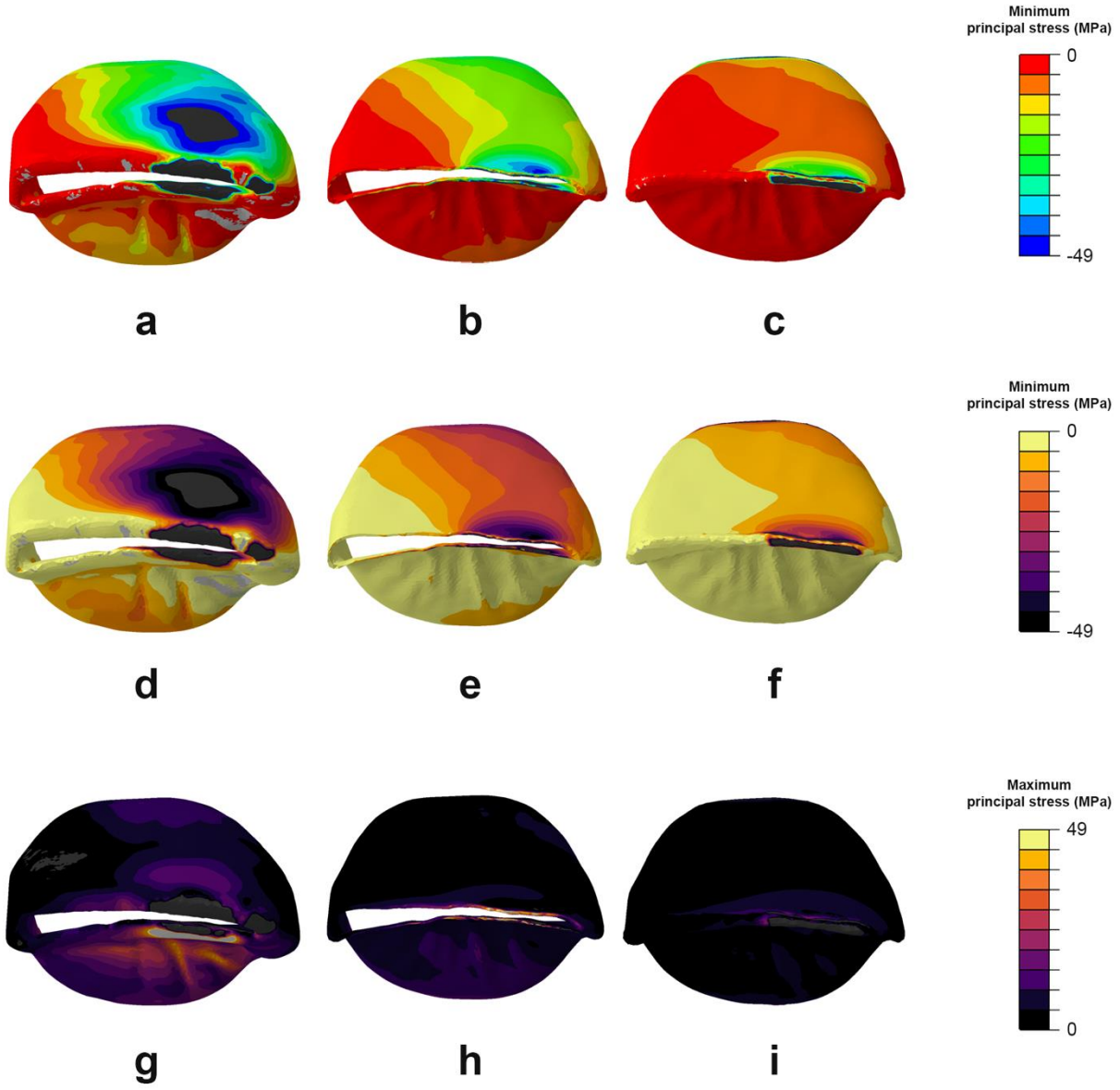

SOM Figure S5. ‘Rainbow’ (a, b, and c) and **‘**inferno’ (d, e, and f) color maps showing the minimum principal stress distribution (MPa) of Le Moustier 1 left I^1 in occlusal view during edge-to-edge occlusion (applied force = 294.4 N). On the bottom, **‘**inferno’ (g, h, and i) color maps showing the maximum principal stress distribution. Enamel (a, d, and g), enamel-dentine junction (b, e, and h) and dentine (c, f, and i).

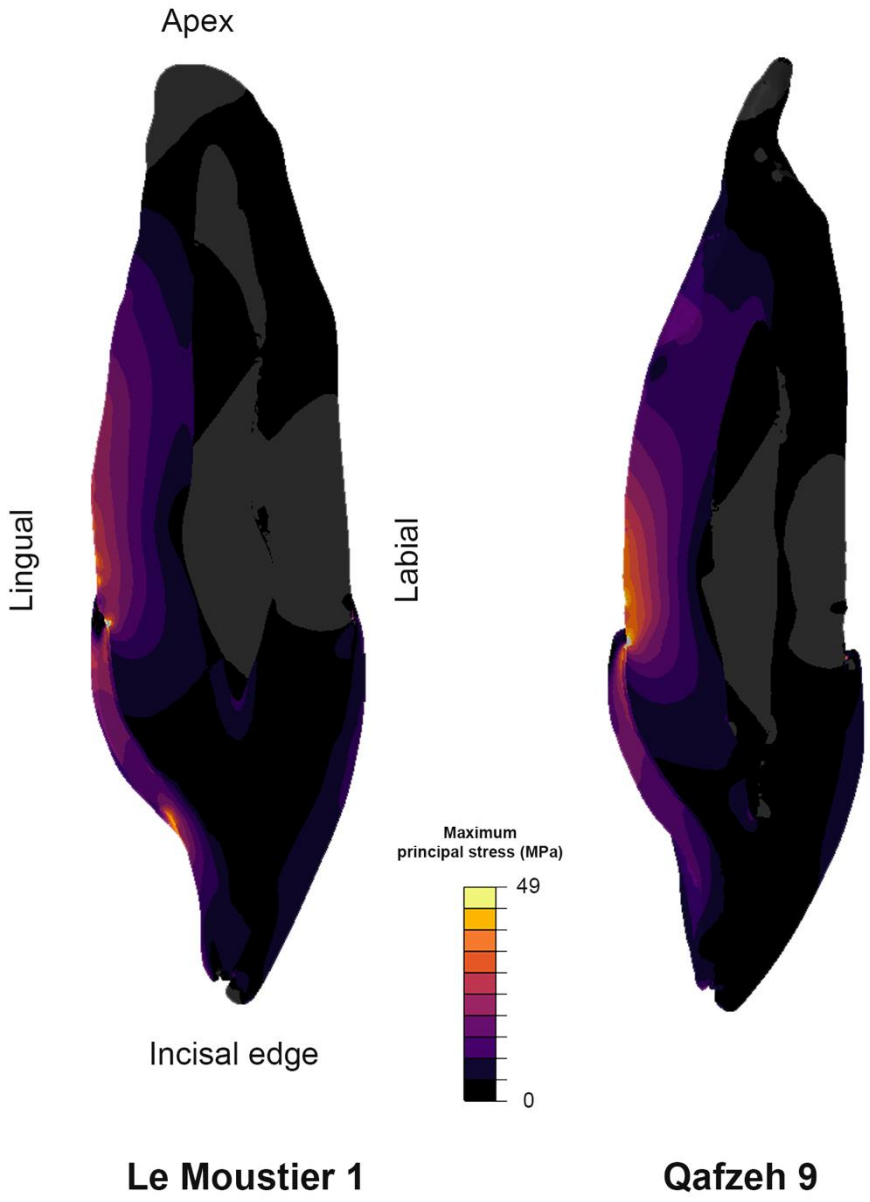

SOM Figure S6. 'Rainbow' color maps showing the maximum principal stress distribution (MPa) of Le Moustier 1 (applied force = 294.4 N) and Qafzeh 9 (applied force = 188 N) left I^1 in midsagittal view during edge-to-edge occlusion.

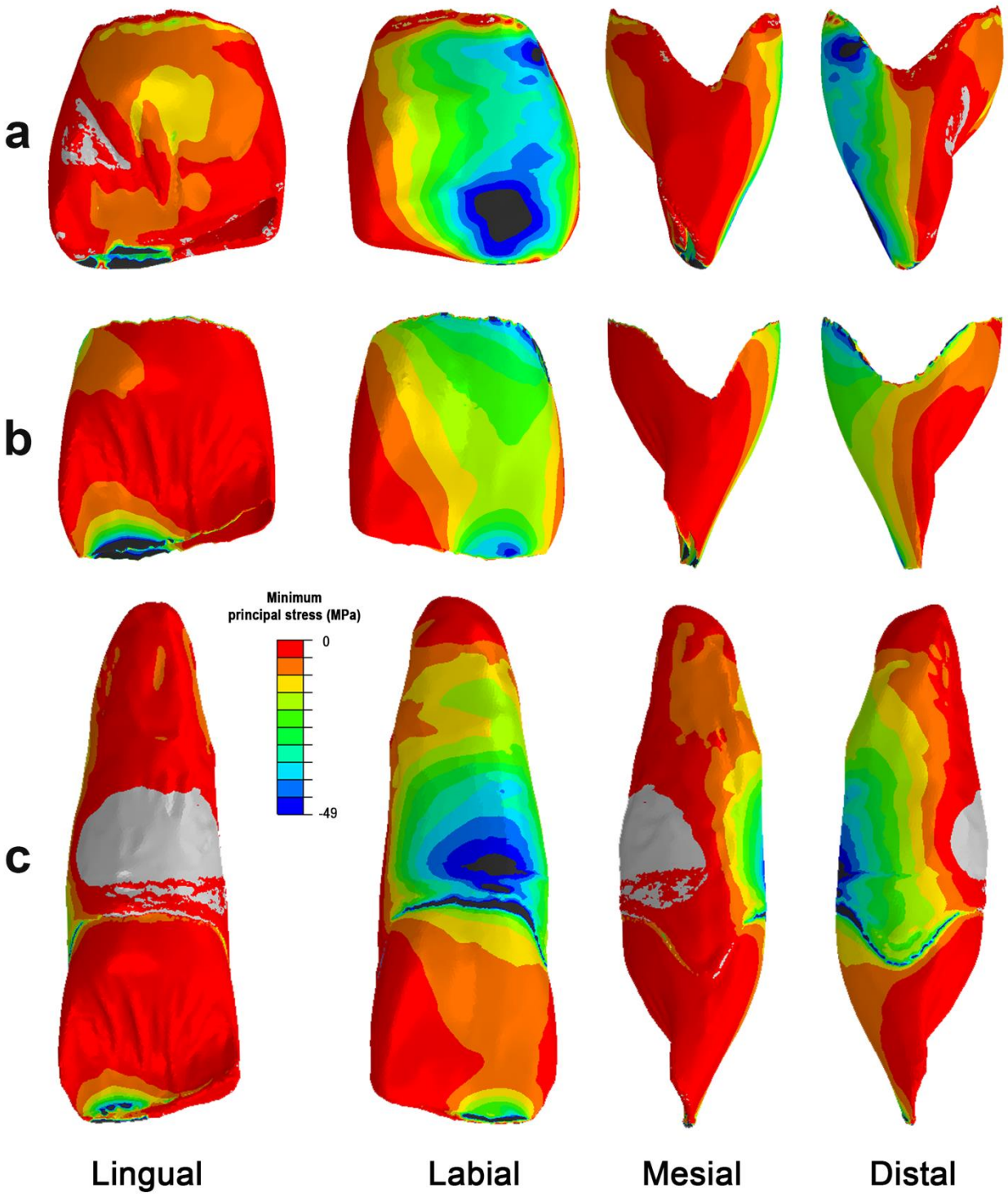

SOM Figure S7. Minimum principal stress distribution (MPa) of Le Moustier 1 left I^1 in lingual, labial, mesial and distal view during edge-to-edge occlusion (applied force = 294.4 N). Enamel (a),

enamel-dentine junction (b) and dentine (c).

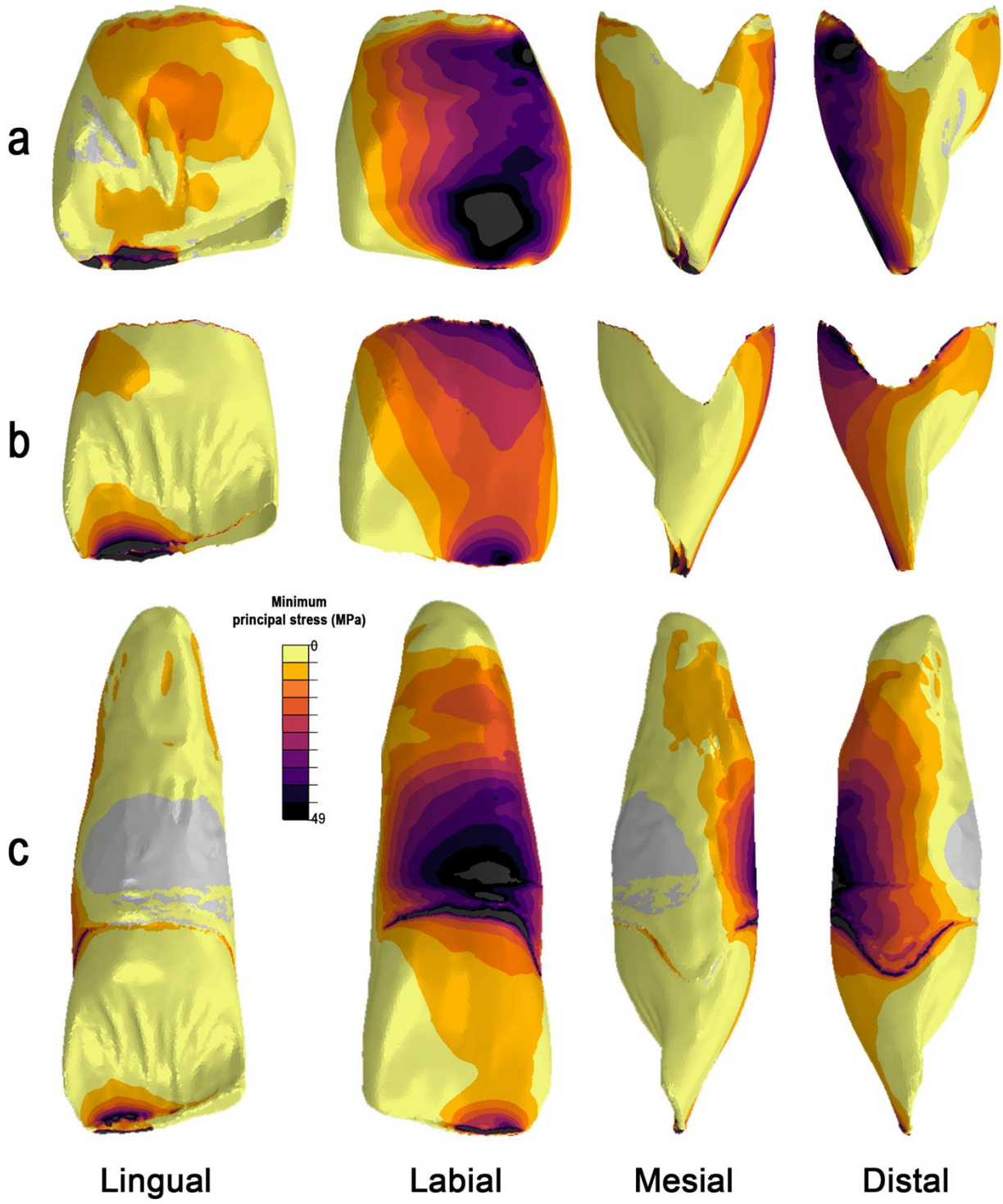

SOM Figure S8. 'Inferno' color maps showing the minimum principal stress distribution (MPa) of Le Moustier 1 left I^1 in lingual, labial, mesial and distal view during edge-to-edge occlusion (applied force = 294.4 N). Enamel (a), enamel-dentine junction (b) and dentine (c).

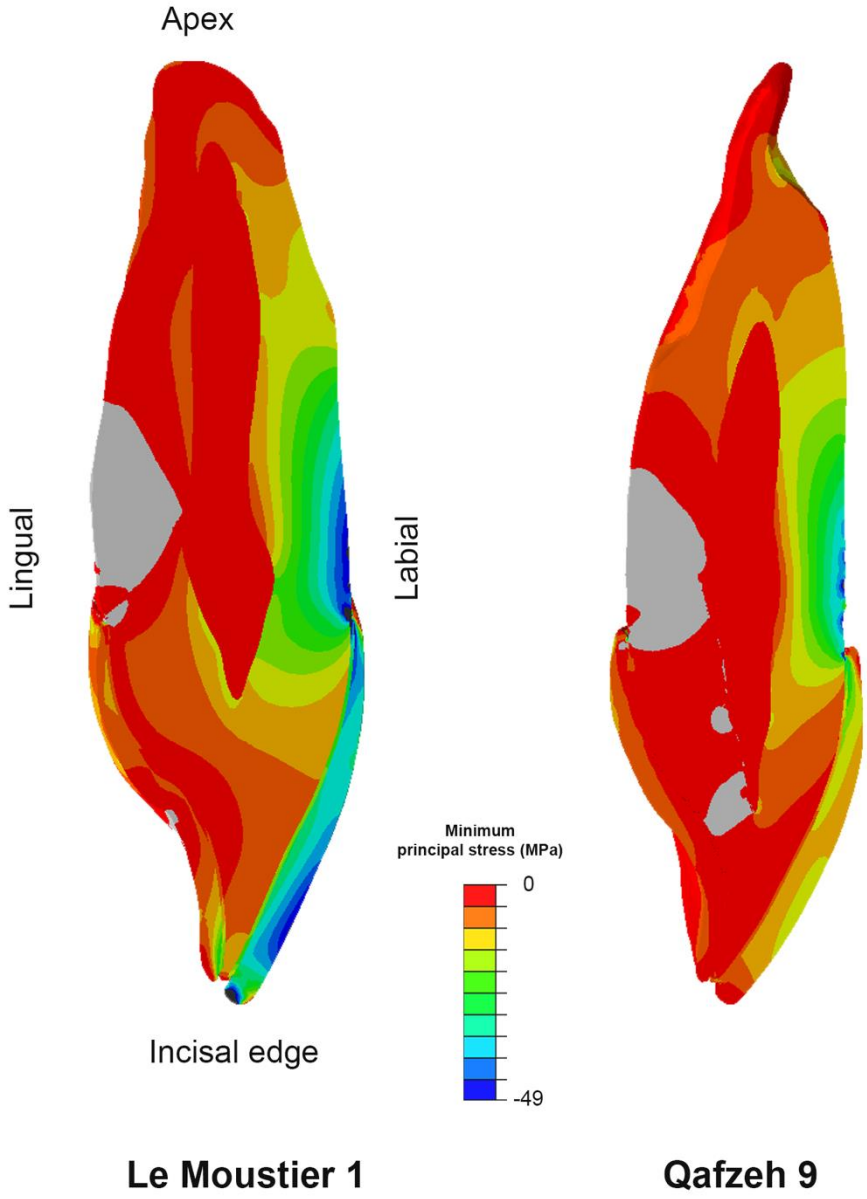

SOM Figure S9. Minimum principal stress distribution (MPa) of Le Moustier 1 (applied force = 294.4 N) and Qafzeh 9 (applied force = 188 N) left I^1 in midsagittal view during edge-to-edge occlusion.

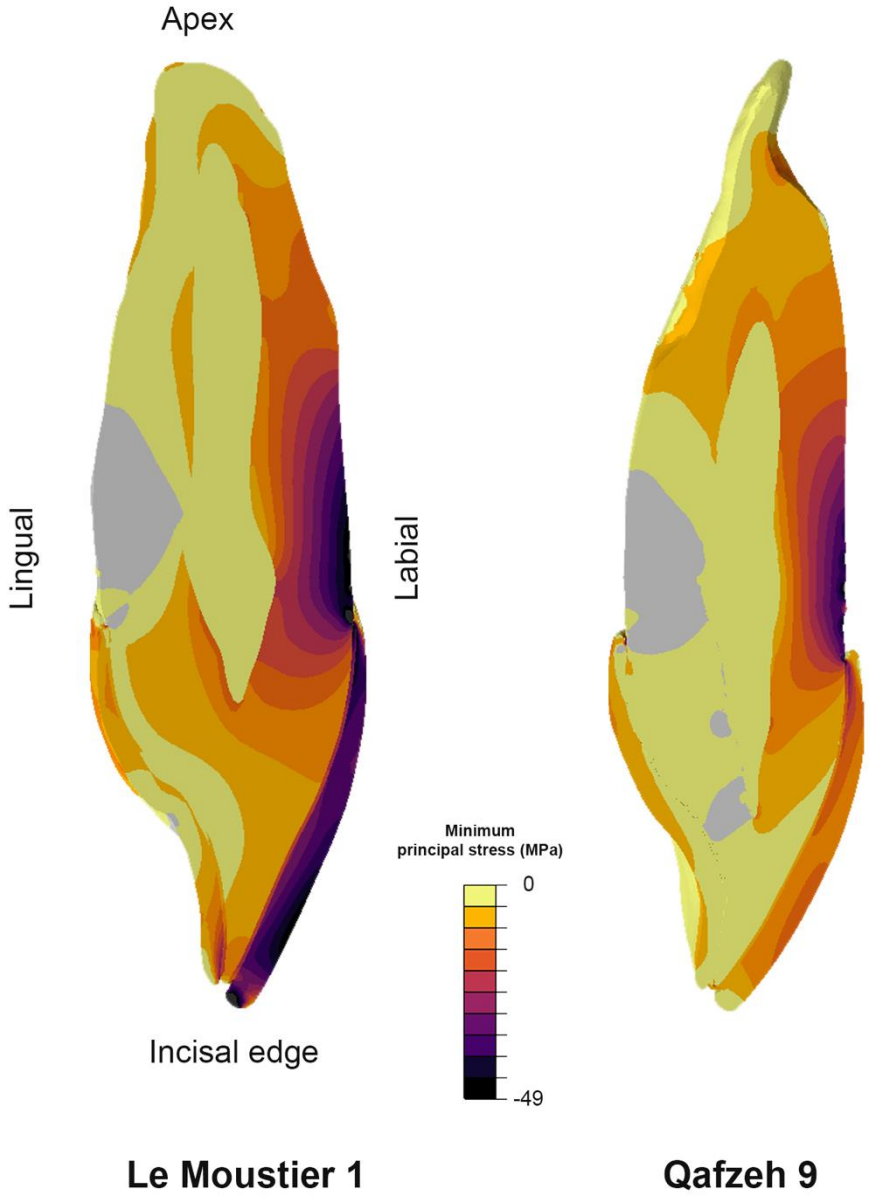

SOM Figure S10. 'Rainbow' color maps showing the minimum principal stress distribution (MPa) of Le Moustier 1 (applied force = 294.4 N) and Qafzeh 9 (applied force = 188 N) left I^1 in midsagittal view during edge-to-edge occlusion.

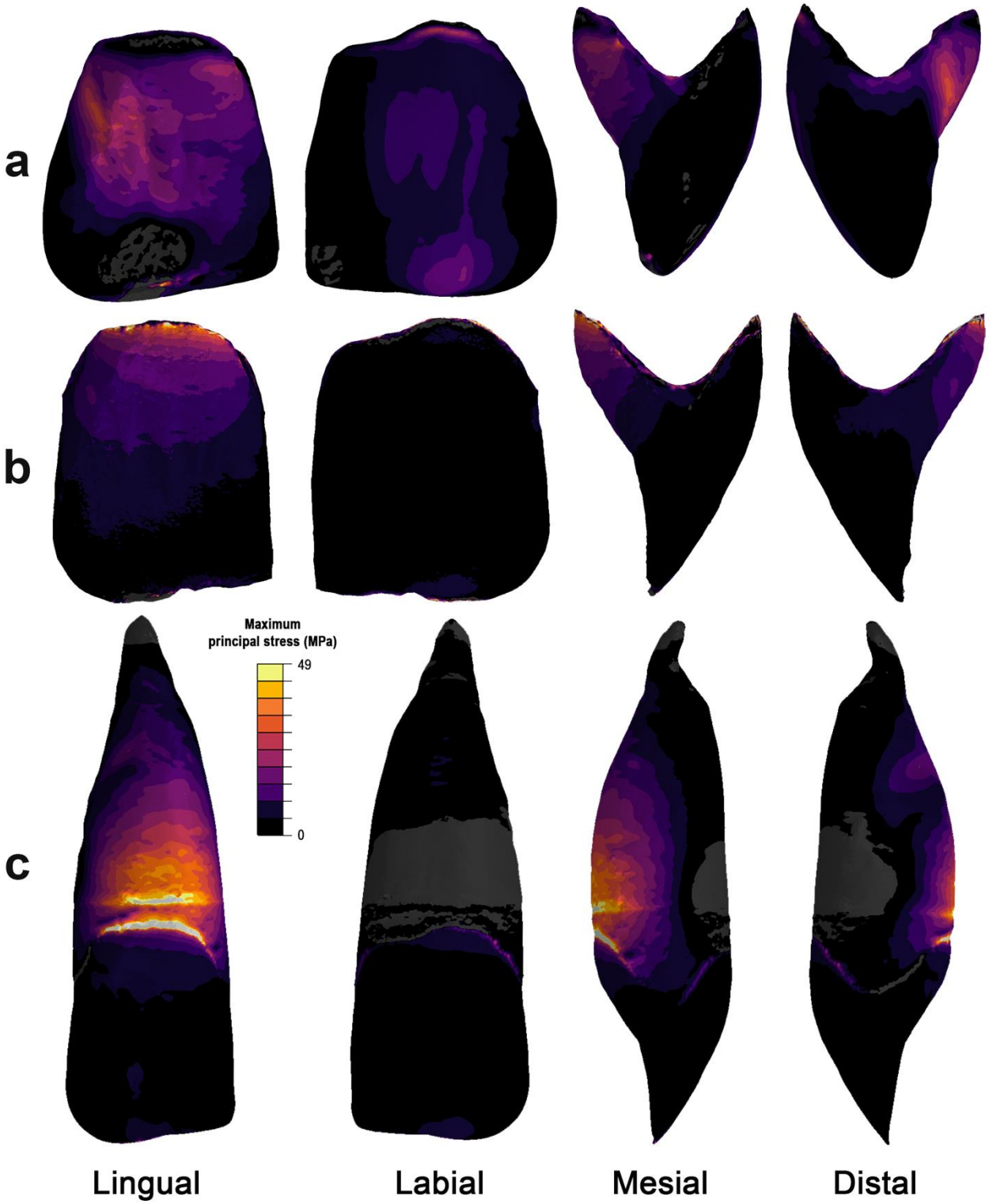

SOM Figure S11. 'Inferno' color maps showing the maximum principal stress distribution (MPa) of Qafzeh 9 left I^1 in lingual, labial, mesial and distal view during edge-to-edge occlusion (applied force = 188 N). Enamel (a), enamel-dentine junction (b) and dentine (c).

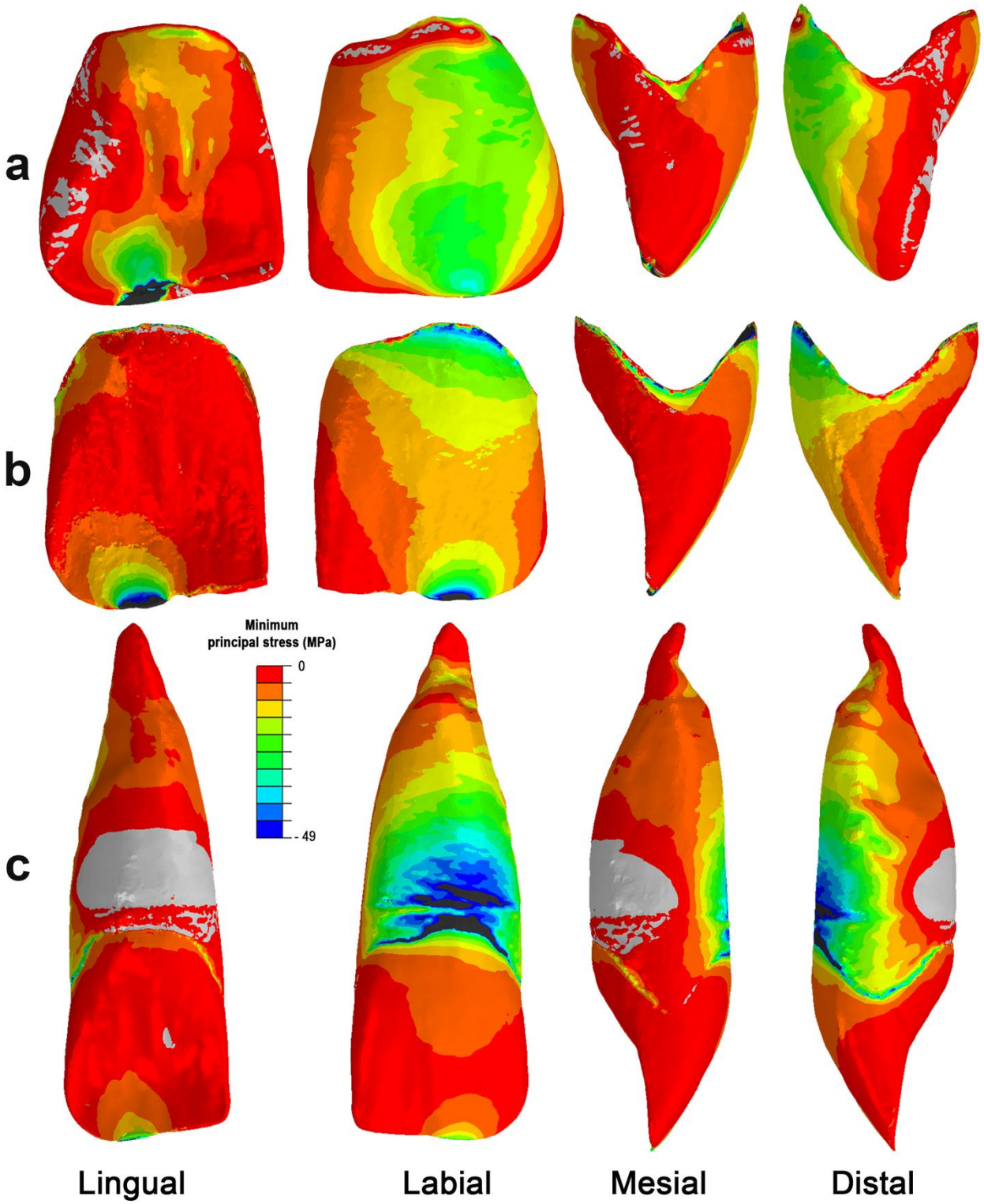

SOM Figure S12. Minimum principal stress distribution (MPa) of Qafzeh 9 left I^1 in lingual, labial, mesial and distal view during edge-to-edge occlusion (applied force = 188 N). Enamel (a), enamel-dentine junction (b) and dentine (c).

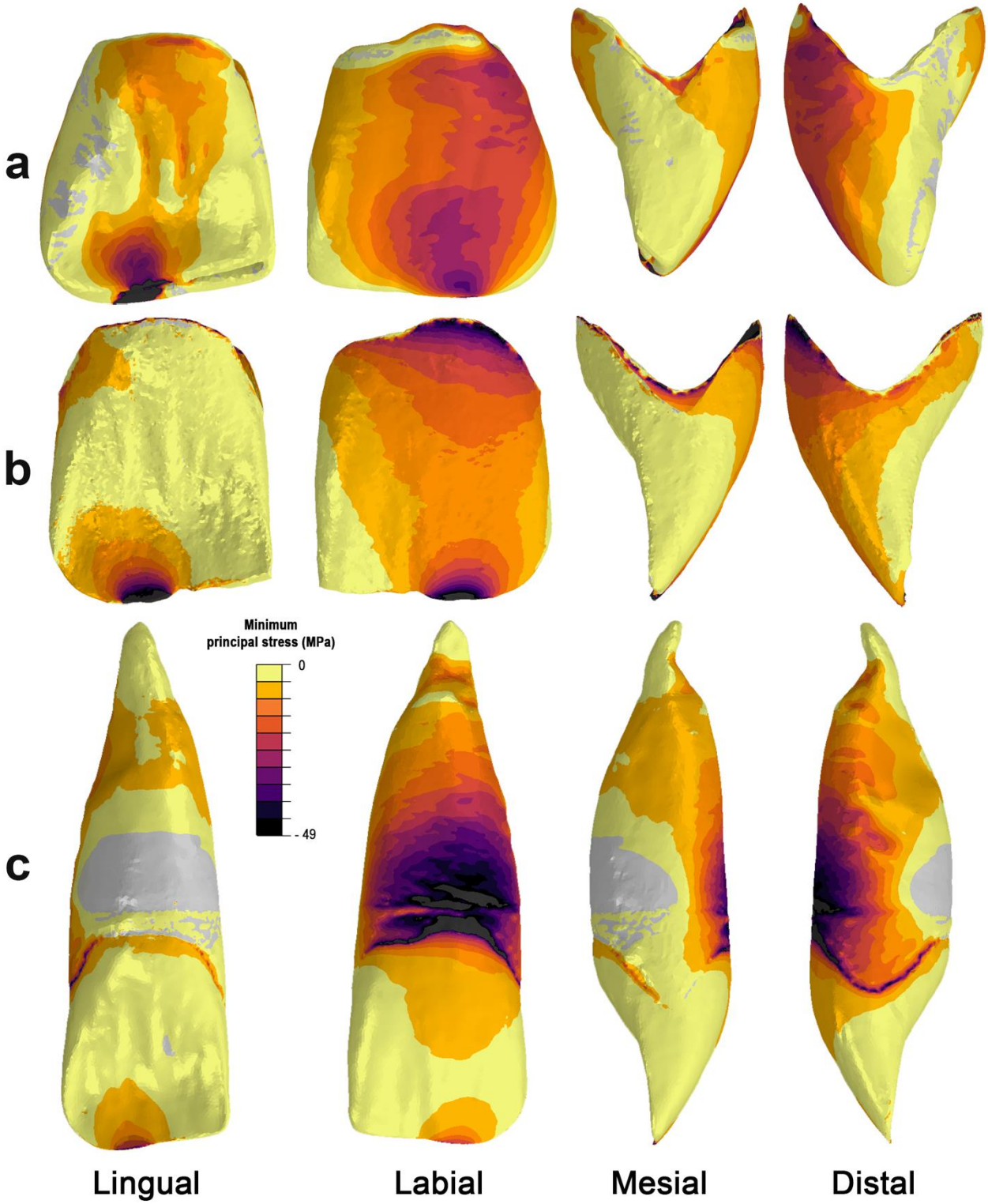

SOM Figure S13. 'Inferno' color maps showing the minimum principal stress distribution (MPa) of Qafzeh 9 left I^1 in lingual, labial, mesial and distal view during edge-to-edge occlusion (applied force = 188 N). Enamel (a), enamel-dentine junction (b) and dentine (c).

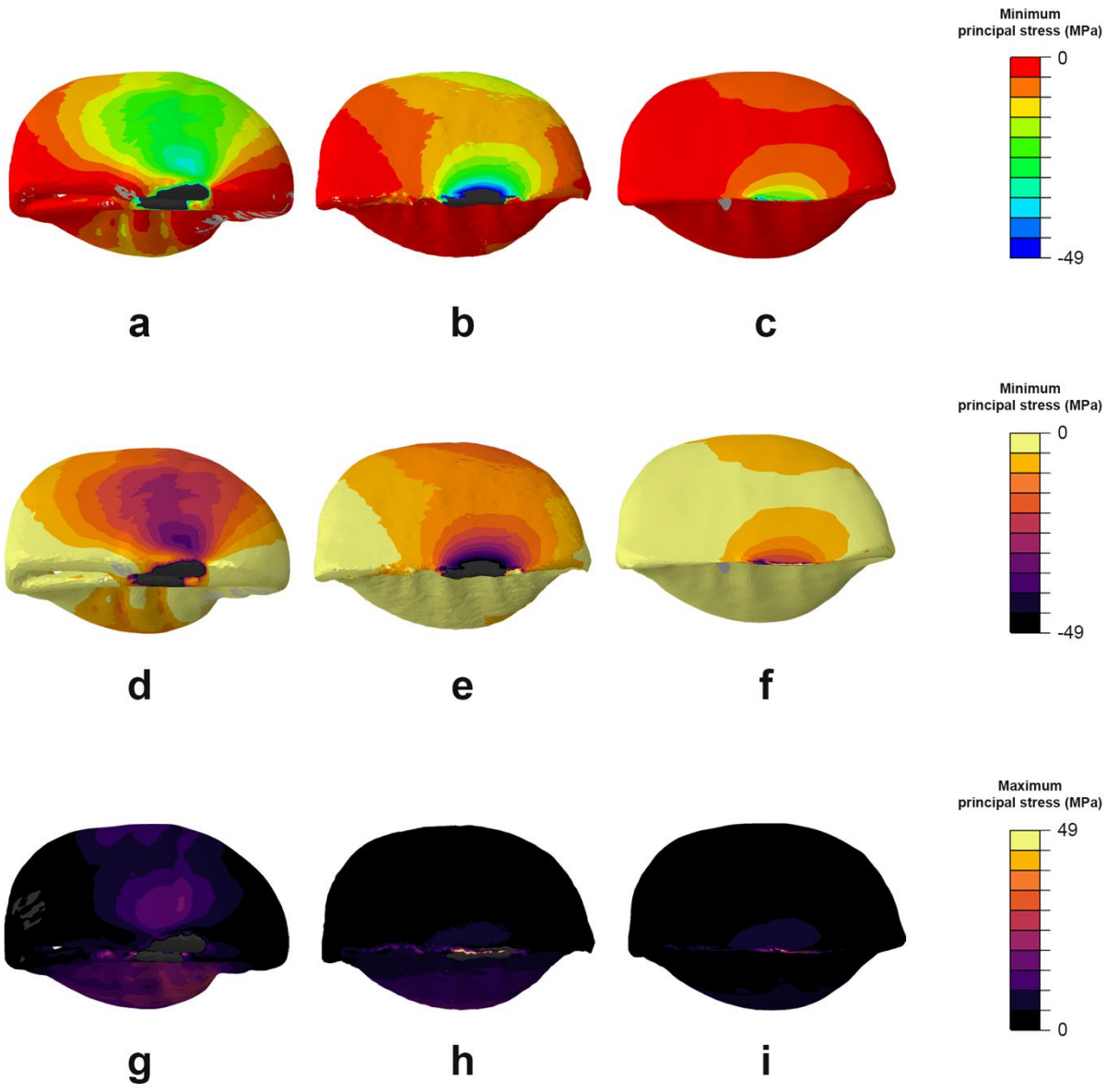

SOM Figure S14. ‘Rainbow’ (a, b, and c) and **‘**inferno’ (d, e, and f) color maps showing the minimum principal stress distribution (MPa) of Qafzeh 9 1 left I^1 in occlusal view during edge-to-edge occlusion (applied force = 188 N). On the bottom, **‘**inferno’ (g, h, and i) color maps showing the maximum principal stress distribution. Enamel (a, d, and g), enamel-dentine junction (b, e, and h) and dentine (c, f, and i).

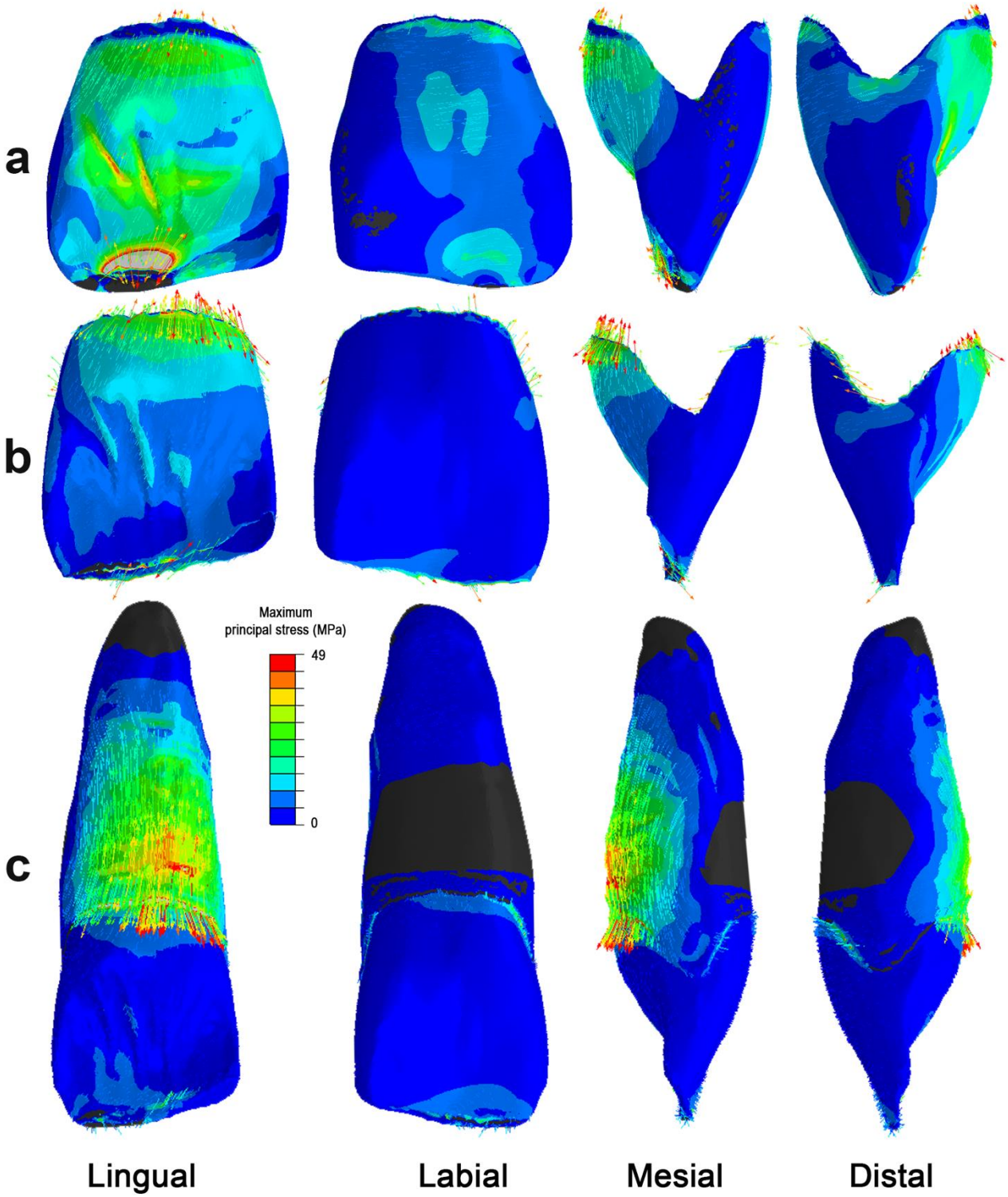

SOM Figure S15. Vector plots showing the orientation of maximum principal stress distribution (MPa) of Le Moustier 1 left I^1 in lingual, labial, mesial and distal view during edge-to-edge occlusion (applied force = 294.4 N). Enamel (a), enamel-dentine junction (b) and dentine (c).

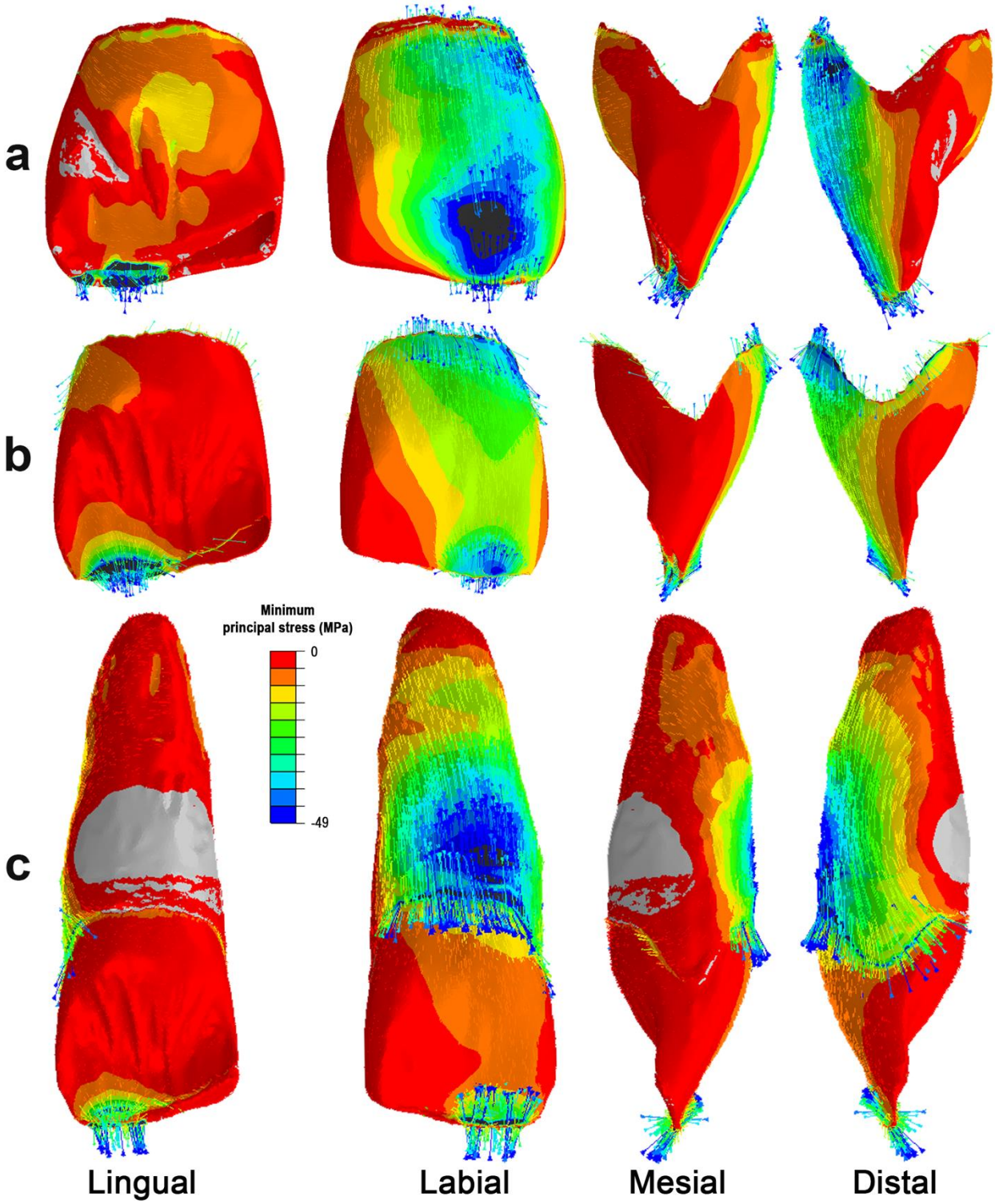

SOM Figure S16. Vector plots showing the orientation of minimum principal stress distribution (MPa) of Le Moustier 1 left I^1 in lingual, labial, mesial and distal view during edge-to-edge occlusion (applied force = 294.4 N). Enamel (a), enamel-dentine junction (b) and dentine (c).

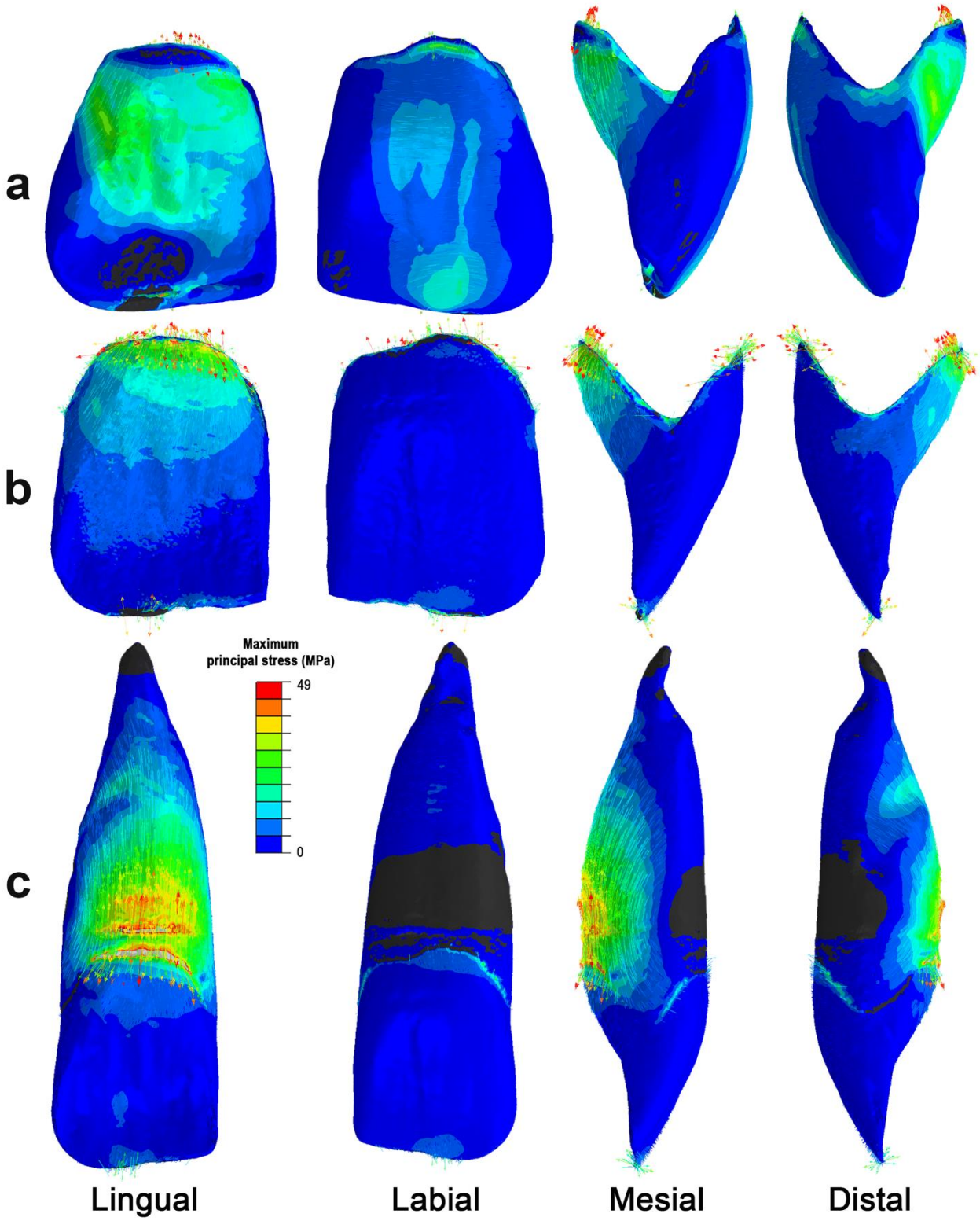

SOM Figure S17. Vector plots showing the orientation of maximum principal stress distribution (MPa) of Qafzeh 9 left I^1 in lingual, labial, mesial and distal view during edge-to-edge occlusion (applied force = 188 N). Enamel (a), enamel-dentine junction (b) and dentine (c).

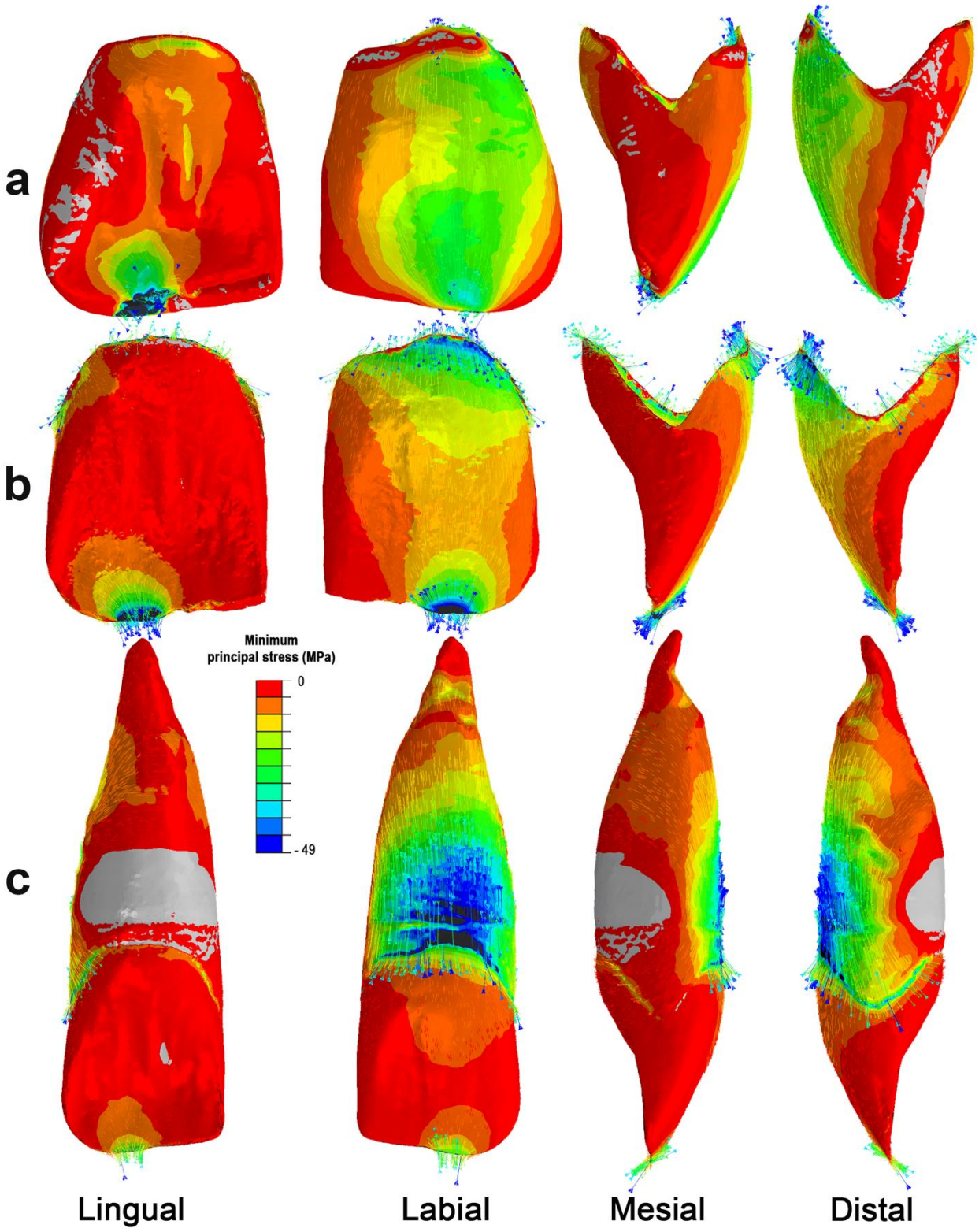

SOM Figure S18. Vector plots showing the orientation of minimum principal stress distribution (MPa) of Qafzeh 9 left I^1 in lingual, labial, mesial and distal view during edge-to-edge occlusion (applied force = 188 N). Enamel (a), enamel-dentine junction (b) and dentine (c).

SOM Table S1

Qualitative analysis of dental non-metric traits based on the Arizona State University Dental Anthropology System (ASUDAS; Turner II et al., 1991).

ASUDAS	Le Moustier 1 Expression	Qafzeh 9 Expression	Range of expression
Curvature	2	0	0-4
Shoveling	1	0	0-6
Double shoveling	0	1	0-6
Lingual tuberculum	3	1	1-4

SOM Table S2

Elastic properties of isotropic materials.

Materials	E[a] (GPa)	Poisson's ratio	References
Enamel	84.100	0.300	Magne (2007)
Dentine	18.600	0.310	Ko et al. (1992)
EDJ[a]	51.350	0.305	Average between enamel and dentine
Pulp	0.002	0.450	Rubin et al. (1983)
PDL[b]	0.069	0.450	Holmes et al. (1996)
Alveolar bone	11.500	0.300	Dejak et al. (2007)
Cortical bone	13.700	0.300	Ko et al. (1992)

Abbreviations: EDJ = enamel-dentine junction; PDL = periodontal ligament.

[a] Elastic modulus.

SOM Table S3

Values of the components of the three-dimensional enamel thickness of maxillary central incisor in Le Moustier 1, Qafzeh 9, Neanderthal, fossil *Homo sapiens* and in recent *Homo sapiens*. The missing enamel in Qafzeh 9 and Le Moustier 1 left I^1 have been reconstructed following the method shown in O'Hara and Guatelli-Steinberg (2022).[a]

n	Specimen/group	3D enamel volume (mm^3)	Dentine and pulp volume (mm^3)	EDJ surface area (mm^2)	2D AET (mm)	2D RET (scale-free)	3D AET (mm)	3D RET (scale-free)
1	Le Moustier 1	139.48	268.93	214.06	0.65	7.29	0.65	10.09
1	Qafzeh 9	205.86	304.54	247.35	0.76	10.67	0.83	12.37
5	Neanderthal				0.63	9.19		
2	Fossil *H. sapiens*				0.71	10.57		
32	Recent *H. sapiens*				0.62	10.91		

Abbreviations: 3D = three-dimensional; EDJ = enamel-dentine junction; 2D = bidimensional; AET = average enamel thickness; RET = relative enamel thickness.

[a] 2D AET and 2D RET values of Neanderthal, recent and fossil *Homo sapiens* taken from Smith et al. (2012).

SOM References

Dejak, B., Mlotkowski, A., Romanowicz, M., 2007. Strength estimation of different designs of ceramic inlays and onlays in molars based on the Tsai-Wu failure criterion. J. Prosthet. Dent. 98, 89–100.

Holmes, D.C., Diaz-Arnold, A.M., Leary, J.M., 1996. Influence of post dimension on stress distribution in dentin. J. Prosthet. Dent. 75, 140–147.

Ko, C.C., Chu, C.S., Chung, K.H., Lee, M.C., 1992. Effects of posts on dentin stress distribution in pulpless teeth. J. Prosthet. Dent. 68, 421–427.

Lee, J.J.-W., Morris, D., Constantino, P.J., Lucas, P.W., Smith, T.M., Lawn, B.R., 2010. Properties of tooth enamel in great apes. Acta Biomat. 6, 4560-4565.

Magne, P., 2007. Efficient 3D finite element analysis of dental restorative procedures using micro-CT data. Dent. Mat. 23, 539-548.

O'Hara, M.C., Guatelli-Steinberg., D., 2022. Reconstructing tooth crown heights and enamel caps: A comparative test of three existing methods with recommendations for their use. Anat. Rec. 305, 123–143.

Rubin, C., Krishnamurthy, N., Capilouto, E., Yi, H., 1983. Stress analysis of the human tooth using a three-dimensional finite element model. J. Dent. Res. 62, 82–86.

Smith, T.M., Olejniczak, A.J., Zermeno, J.P., Tafforeau, P., Skinner, M.M., Hoffmann, A., Radovčić, J., Toussaint, M., Kruszynski, R., Menter, C., Moggi-Cecchi, J., Glasmacher, U.A., Kullmer, O., Schrenk, F., Stringer, C., Hublin, J.-J., 2012. Variation in enamel thickness within the genus *Homo*. J. Hum. Evol. 62, 395–411.

Turner, C.G., II, Nichol, C. R., Scott, G., 1991. Scoring procedures for key morphological traits of the permanent dentition: The Arizona State University dental anthropology system. In: M. Kelley, M., Larsen, C. (Eds.), Advances in Dental Anthropology. Wiley Liss, New York, pp. 13-31.